Journal of Power Sources 241 (2013) 429–439

Contents lists available at SciVerse ScienceDirect

Journal of Power Sources

journal homepage: www.elsevier.com/locate/jpowsour

Hydrogenotitanates nanotubes supported platinum anode for direct methanol fuel cell

Bochra Abida [a,*], Lotfi Chirchi [a], Stève Baranton [b], Teko Wilhelmin Napporn [b], Cláudia Morais [b], Jean-Michel Léger [b], Abdelhamid Ghorbel [a]

[a] Laboratoire de Chimie des Matériaux et Catalyse, Faculté des Sciences de Tunis, Campus Universitaire El-Manar 2092, El-Manar, Tunisia
[b] IC2MP, UMR 7285, CNRS-Université de Poitiers, 4, rue Michel Brunet B27, 86022 Poitiers, France

HIGHLIGHTS

- HTNs as a support for catalysts.
- In situ infrared reflectance spectroscopy measurements of different catalysts.
- For methanol oxidation, Pt/HTNs have high current density.

GRAPHICAL ABSTRACT

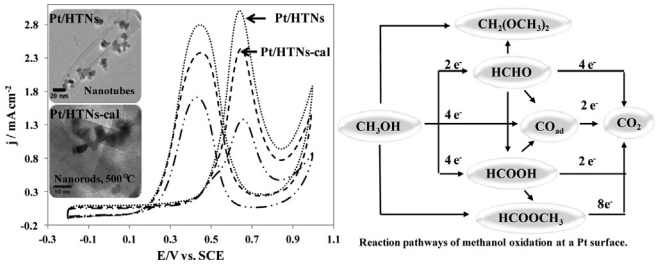

ARTICLE INFO

Article history:
Received 8 January 2013
Received in revised form
17 April 2013
Accepted 21 April 2013
Available online 9 May 2013

Keywords:
Hydrogenotitanates nanotubes
Platinum nanoparticles
CO stripping
Methanol oxidation
Direct methanol fuel cell

ABSTRACT

Hydrogenotitanates nanotubes (HTNs) are prepared from TiO_2 powder via hydrothermal processing in 11.25 M NaOH aq. The reaction temperature is 130 °C for 20 h. Afterward a heat treatment is done during 2 h at 500 °C in air, to obtain calcined HTNs (HTNs-cal). The structural change on the molecular TiO_2 during the hydrothermal treatment is investigated in detail by various analytic techniques such as XRD and TEM, which reveal that the crystal structure of the HTNs materials is similar to that of $H_2Ti_2O_5 \cdot H_2O$ nanotubes with 160 nm in length and 10 nm in diameter. Nitrogen adsorption–desorption isotherms indicate that synthesized solids are mesoporous materials with a multiwalled nanotubular structure and high specific surface area. Platinum nanoparticles are deposited on the HTNs by the impregnation method for a total noble metal loading of 10 wt%. The electrocatalytic activity of these electrocatalysts is evaluated by cyclic voltammetry in acid medium. Typical CO stripping voltammetry in acidic solutions is investigated. The results demonstrate that the HTNs can greatly enhance the catalytic activity of Pt for methanol oxidation. The CO stripping test shows that the Pt/HTNs can shift the CO oxidation potential to lower direction than Pt/C (XC72) and Pt/HTNs-cal catalysts.

1. Introduction

Direct methanol fuel cell (DMFC) has received extensive studies in the two past decades because of its great application potential as an alternative power source. DMFCs can operate at low temperatures, have a high energy density, a long lifetime and are lightweight with a simple system design [1–6]. As far as the methanol oxidation reaction (MOR) is concerned at the anode, major challenges receiving particular attention are for minimizing the Pt catalyst loading and keeping higher electrocatalytic activities with a better tolerance against the adsorbed CO poisoning effect formed during methanol dissociative adsorption. The widely adopted method to improve the electrocatalytic mass activity of the Pt catalyst toward MOR is to disperse Pt nanoparticles on a large

* Corresponding author. Tel.: +216 71 88 34 24.
E-mail address: abidabochra@yahoo.fr (B. Abida).

0378-7753/$ – see front matter © 2013 Elsevier B.V. All rights reserved.
http://dx.doi.org/10.1016/j.jpowsour.2013.04.090

surface area support [7–9]. On the other hand, to improve the CO_{ads} tolerance, numerous studies used Pt-based binary or ternary catalysts (as Pt–Ru, Pt–Sn) to enhance CO_{ads} electro-oxidation via the bifunctional mechanism and the so-called electronic effect [10–12].

Usually, carbon powder is used as support for these electrocatalysts. However, during the long-term operation of these electrocatalysts, a corrosion phenomenon was observed leading to a decrease of their activity and a deterioration of the system performance. Effort was made for improving the stability of carbon or to find an alternative stable material as support. In previous studies, nanocrystalline metal-oxide semiconductors have been widely employed in photocatalytic or photoelectrochemical systems because of the large area of the solid–solution interface, where the interactions between the photon-induced charge carriers and the active species in the solution [13,14]. Among these semiconductors, TiO_2 has drawn much attention, and numerous efforts have been devoted to the synthesis of nanosized TiO_2. Kasuga et al. [15] reported that the thermal treatment of TiO_2 particles in NaOH resulted in the formation of anatase TiO_2 nanotubes with large surface areas. Apart from the crystalline structure of anatase TiO_2 nanotubes, some titanate structures, such as $A_2Ti_2O_5 \cdot H_2O$ [16], $A_2Ti_3O_7$ [17,18], $H_2Ti_4O_9 \cdot H_2O$ [19], and lepidocrocite titanates [20], have been assigned as nanotubes constituents (A = Na and/or H). Studies carried out on commercial Pt/C catalysts mixed with titanium dioxide nanotubes for direct alcohol fuel cells have shown that the presence of titanium dioxide nanotubes improved the catalytic performance of Pt/C [21,22].

In this study, the hydrogenotitanates nanotubes (HTNs) were synthesized through the dissolution of TiO_2 powders in high concentrated NaOH solution at a high reaction temperature and then treated with hydrochloric acid or water. Their tubular structure showed a larger surface area and a higher degree of porosity than that of hydrogenotitanates nanotubes calcinated at 500 °C, and an improvement of the electrochemical activity was evidenced. Furthermore, a strong interaction has been reported in the case of platinum catalysts dispersed on hydrogenotitanates nanotubes leading to an improvement of the electrocatalytic activity of platinum when compared with platinum dispersed on other substrates.

In this paper, we will present recent progress made in the understanding of the mechanisms of the methanol oxidation reaction at Pt/HTNs catalyst by in situ infrared reflectance spectroscopy. The catalysts were characterized by Nitrogen adsorption–desorption isotherms (N_2 adsorption–desorption), X-ray diffraction (XRD), and transmission electron microscopy (TEM). Their electrocatalytic activities were evaluated through the methanol oxidation by cyclic voltammetry and in situ reflectance infrared spectro-electrochemical measurements (FTIR).

2. Experimental

2.1. Preparation of hydrogenotitanates nanotubes by hydrothermal process

Hydrogenotitanates nanotubes were prepared by hydrothermal method similar to that described by Kasuga et al. [15]. In a typical procedure, 0.5 g of TiO_2 (Degussa P25) were dispersed in an aqueous solution of 11.25 M NaOH (15 mL) and placed in a Teflon-lined stainless-steel autoclave. The autoclave was statically heated at 130 °C for 20 h. After the hydrothermal treatment, one proceeded to the first filtration with one liter of distilled water (at approximately 80 °C) and to a neutralization with 0.1 M of a hydrochloric acid solution (HCl) until pH = 7. After this neutralization, a second washing with 0.5 L ebullient water was carried out, followed by a filtration and finally by a drying at 80 °C for 24 h. HTNs were obtained. Finally, HTNs were calcinated at 500 °C under air for 2 h (HTNs-cal).

2.2. Preparation of Pt nanoparticles

The platinum nanoparticles where synthesized using the impregnation method. In order to produce 10 wt% Pt/substrate catalysts, 0.5 g of substrate (carbon Vulcan XC72, HTNs or HTNs-cal) was mixed with 6.25 mL of hexachloroplatinic acid solution (20 g L^{-1}). The mixture was ultrasonically treated for 30 min and stirred for 2 h. Then 200 mL of 0.4 M $NaBH_4$ at 80 °C was added to the mixture under vigorous stirring. The catalytic powder was then filtered and washed with a large amount of water and dried under vacuum at 110 °C for 4 h.

2.3. Characterization of catalysts

The morphology of the prepared catalyst was investigated by transmission electron microscopy (TEM). The sample specimens for TEM experiment were prepared by dispersing the catalyst powder in ethanol by ultrasonic treatment for 15 min, dropping onto a carbon film supported by a copper grid. TEM images were obtained using instrument a JEOL JEM-2001 LaB_6 microscope with an accelerating voltage of 200 kV and a resolution of ca. 0.19 nm. X-ray diffraction (XRD) analysis was performed using a "Philips analytical" X-ray diffractometer with Cu Kα radiation. The 2θ angular regions between 2° and 70° were explored at a scan rate of 6° min^{-1} with step of 0.02°.

The Brunauer–Emmett–Teller (BET) equation was used to calculate the specific surface area (S_{BET}). Mean pore diameter (d_p) was obtained using the Barrett–Joyner–Halenda (BJH) model in the range of mesopores. Pore distribution of the HTNs and S_{BET} were calculated from nitrogen adsorption and desorption isotherms at 77 K using a " Micromeritics ASAP 2000 " instrument. 100 mg of HTNs sample was sealed in the reactor equipped with a temperature control unit. The adsorption isotherm was measured at 25 °C using a standard sequence, with a 30 min time out for each point.

Atomic absorption spectroscopy was performed to determine the platinum loading on the supports. An A Analyst 200 atomic absorption Spectrometer (Perkin Elmer) with platinum hollow cathode lamp (λ = 265 nm) was used. The catalytic powder was previously mineralized in a hydrofluoric, hydrochloric and nitric acid solution under microwave activation for 40 min. The excess of hydrofluoric acid is then removed by the addition of H_3BO_3.

The cyclic voltammetry and CO stripping measurements were obtained using an Autolab potentiostat–galvanostat. All the electrochemical measurements were carried out at 25 °C in a thermostated three electrodes cell. All the potentials in this work were related to a reference saturated calomel electrode (SCE). A solution of 0.5 M H_2SO_4 Suprapur sulfuric acid (Merck) was used as the supporting electrolyte and to prepare the methanol solution (1 M CH_3OH + 0.5 M H_2SO_4) for the oxidation activity test. The working electrode was a glassy carbon disk with a 3 mm diameter (geometric surface area, 0.071 cm^2). It was polished with Al_2O_3 powder and washed carefully before the catalyst deposition. Platinum based working electrodes were prepared from Pt/C (Vulcan XC72), Pt/HTNs or Pt/HTNs-cal catalysts. An ink was prepared by ultrasonically dispersing 5 mg catalytic powder with 5 mg of carbon Vulcan XC72 in 0.5 mL 5% wt. Nafion® solution (from Aldrich). The 5 mg of carbon Vulcan XC72 powder were added to Pt/HTNs and Pt/HTNs-cal in order to ensure a good electronic conductivity of the catalytic layer. A drop of 3.0 μL catalyst ink was deposited onto the working electrode surface. Glassy carbon was used as the counter electrode. The reference electrode was separated from the working electrode compartment by an electrolyte bridge. Before the cyclic voltammetry measurements, nitrogen was bubbled in the supporting electrolyte for 30 min at room temperature. Recorded at

50 mV s^{-1} from −0.2 V to 1.1 V *vs.* SCE, 6 cycles of voltammetry were necessary to stabilize the current–potential signal.

Electrochemical methods and in situ reflectance infrared spectro-electrochemical measurements were carried out to determine the electrocatalytic behavior of catalysts based on Pt with HTNs and HTNs-cal supports. The IR measurements were performed in situ under external reflection conditions on a Bruker IFS 66v FTIR spectrometer modified for beam reflection on the electrode surface at a 65° incident angle. To remove interferences from atmospheric water and CO_2 the beam path was vacuum evacuated. A liquid nitrogen-cooled HgCdTe detector was used. Spectra were recorded with data acquisition techniques that enabled the performance of Single Potential Alteration Infrared Reflectance Spectroscopy (SPAIRS) and computed from an average of 256 interferograms. The spectral resolution was set to 4 cm^{-1}. Positive and negative going bands represent respectively the decrease and increase of species. The working electrode consisted of a carbon substrate disc connected to a glass shaft. For each measurement 3.0 μL of the catalytic ink were deposited onto a carbon substrate previously polished with alumina. For infrared in situ experiments, an RHE reference electrode was used.

Measurements were conducted on a small-scale laboratory DMFC with a 5 cm^2 geometric surface area. The anode catalysts were Pt/HTNs (20 wt%), Pt/HTNs-cal (20 wt%) and Pt/C (10 wt%). For the cathode, Pt/C (40 wt%) was used. The membrane electrode assembly (MEA) was fabricated by a hot pressing method for 1 min at 115 °C, 1 t m^{-2}. The anodic compartment was fed with an electrolyte containing 1 M CH_3OH + 0.5 M H_2SO_4 solution and the oxygen flows through the cathodic compartment. Current–voltage curves were obtained at 90 °C.

3. Results and discussion

3.1. TEM analysis of Pt/HTNs and Pt/HTNs-cal

TiO_2 powders have been hydrothermally transformed into hydrogenotitanates nanotubes at 130 °C for 20 h. TEM image in Fig. 1a shows a typical structure of nanotubes [23,24] which are about 50–160 nm in length and 5–10 nm in diameter. They also present a multi-layered structure (2–10 layers), the interlamellar space ranges between 0.25 and 0.8 nm. The dispersion of Pt on the titanium dioxide nanotubes is uniform as depicted in Fig. 1 (b and c). Metal particle sizes were in the range 2–7 nm.

Fig. 2a shows TEM images of HTNs-cal sample, after calcination at 500 °C. The HTNs are transformed into nanorods and presented are very well crystallinized [25]. The lengths were measured to be 40 nm less than that of HTNs. The distance between parallel planes is about 0.5 nm corresponding to the inter-reticular distance d_{110} of the anatase phase. This was also consistent with the XRD results which show that the patterns drastically changed after calcination

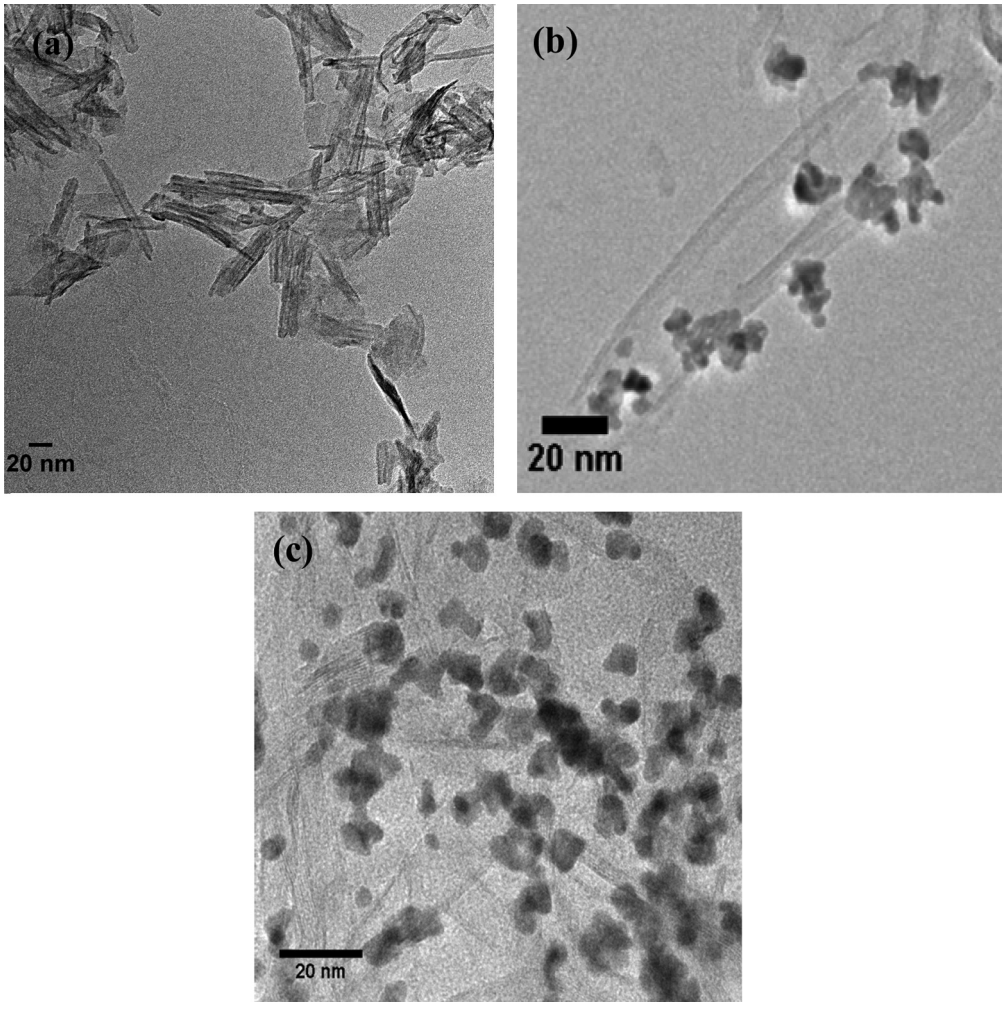

Fig. 1. TEM images of Pt/HTNs.

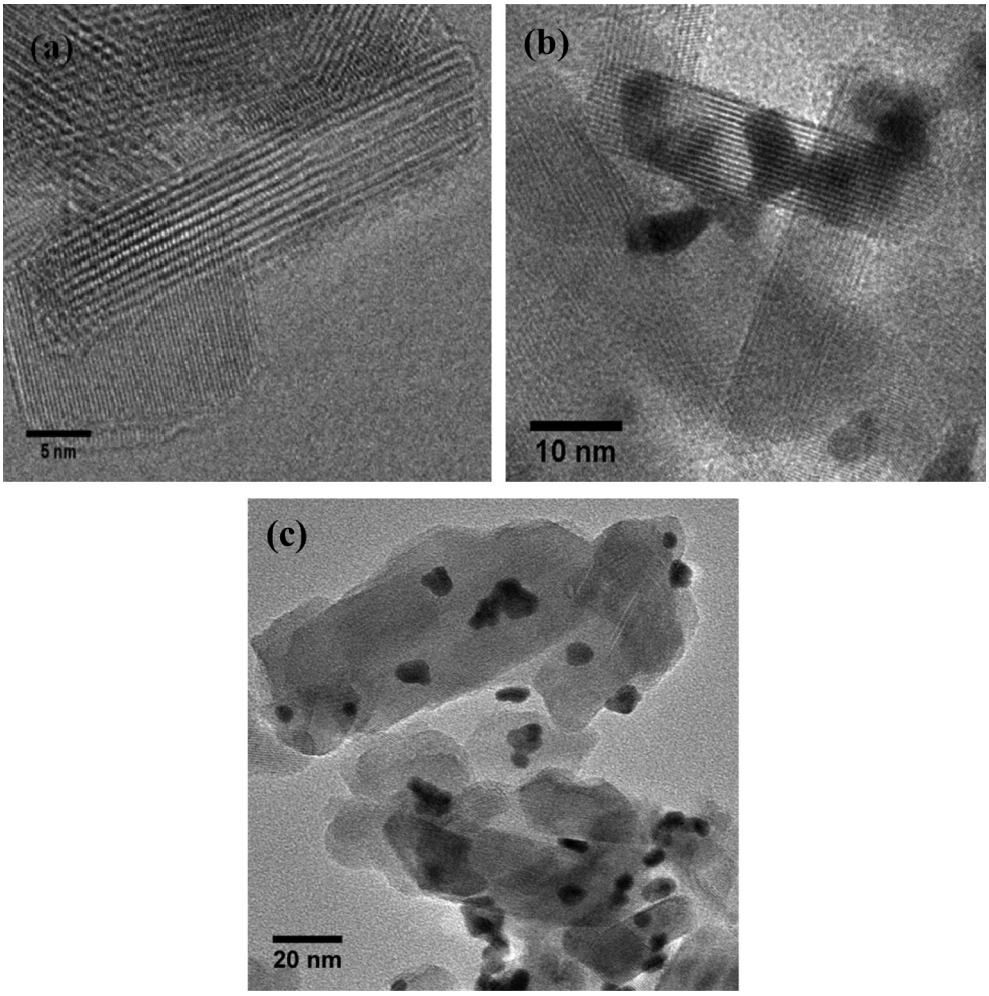

Fig. 2. TEM images of Pt/HTNs-cal.

at 500 °C. The dispersion of Pt on HTNs-cal is uniform as depicted in Fig. 2 (b and c). Metal particle sizes were about 5–10 nm.

3.2. Morphology and structure of Pt/HTNs and Pt/HTNs-cal

In the XRD pattern of the Pt/HTNs catalyst as shown in Fig. 3, the broad reflection peaks were observed at $2\theta = 9.9°$, 24.5°, 28° and 48.5° which reveal the presence of hydrogenotitanates nanotubes "$H_2Ti_2O_5$, H_2O" phase (JCPDS card: 47-0124). The results are illustrated in Table 1. The intensity of the peaks around 9.9° (d_{200}) corresponding to the interlayer spacing, shows an orthorhombic system with the lattice constants $a_0 = 1.926$ nm, $b_0 = 0.378$ nm and $c_0 = 0.300$ nm [26,27].

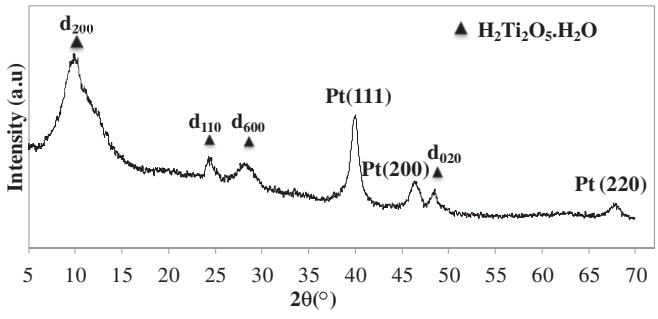

Fig. 3. XRD pattern of Pt/HTNs.

The relative ratio of 110–600 peaks intensities can be used as a measure of sodium content. As shown in Fig. 3 the peak 600 is less intensive than the 110. This suggests a replacement of most of Na^+ ions by H^+ during the washing with HCl 0.1 M [28]. The characteristic XRD peaks of platinum in Fig. 3 can be indexed as the face-centered cubic phase Pt (111), Pt (200) and Pt (220).

After calcination of HTNs at 500 °C, it can be seen from Fig. 4, that the intensities of the peaks around 9.9° (d_{200}) and 24.5° (d_{110}) decreased and shifted to a higher angle value, indicating a decrease in the interlayer distance in this plane. This contraction of layers may be due to the release of water molecules adsorbed and present in the spacing. New peaks appeared showing the transformation of the initial HTNs sample to anatase phase.

Table.1
XRD data of HTNs.

h k l	*d* (A)	2θ (°)	I (%)
200	9.04	9.9	100
110	3.696	24.5	18
600	3.17	28	36
020	1.89	48.5	17

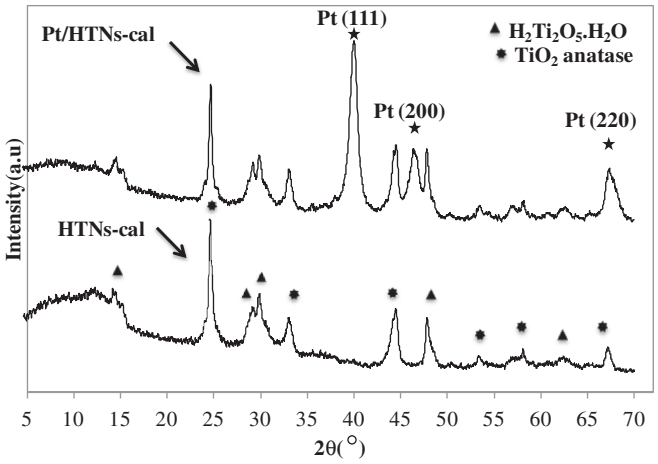

Fig. 4. XRD pattern of Pt/HTNs-cal.

These results reveal that the dehydration process of HTNs is more complex [17]. The dehydration of interlayered OH groups induced the change of crystalline form from orthorhombic system to anatase, while the nanotube morphology was destroyed.

The dehydration reaction of $H_2Ti_2O_5 \cdot H_2O$ consists of two steps which can be illustrated by the following reactions:

$$H_2Ti_2O_5 \cdot H_2O \rightarrow H_2Ti_2O_5 + H_2O \quad (1)$$

$$H_2Ti_2O_5 \rightarrow 2TiO_2 + H_2O \quad (2)$$

From the XRD pattern of the Pt/HTNs-cal catalyst, it can be seen from Fig. 4 new diffraction peaks appear, which are in good agreement with the peaks of Pt nanoparticles and correspond to the face-centered cubic (fcc) crystal structure.

3.3. Textural properties and elemental analysis

The adsorption–desorption isotherm of nitrogen on HTNs and HTNs-cal at 77 K (Fig. 5) is of type IV isotherms with type H3 hysteresis loops. According to the classification of the IUPAC [29], the initial part of the Type IV isotherm is attributed to monolayer-multilayer adsorption. Hysteresis appearing in the multilayer range of physisorption isotherms is usually associated with capillary condensation in mesoporous structures. The Type H3 loop is observed with aggregates of plate-like particles giving rise to slit-shaped pores. Taking into consideration that HTNs are multiwalled scrolls which are believed to be formed through sheet folding or wrapping mechanism, it seems to be reasonable that they exhibit the H3 loop.

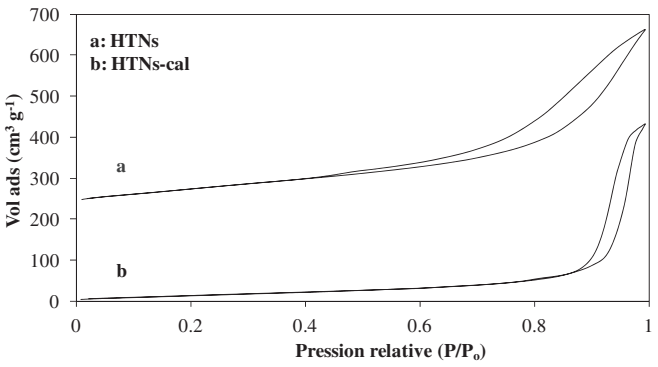

Fig. 5. Adsorption–desorption isotherms of nitrogen at 77 K for (a) HTNs and (b) HTNs-cal.

The effect of calcination temperature on the pore size distribution, mesoporous volume and surface area has been investigated and the results are illustrated in Table 2. When P25 transforms into the HTNs, there is a significant increase for S_{BET} from 43 to 246 $m^2 g^{-1}$ respectively, ascribing to the formation of nanotube structure. However, calcination of the HTNs sample led to a decrease in surface area to 60 $m^2 g^{-1}$. This decrease can be explained by the disappearance of the multiwalled structure and partial agglomeration on the nanorods. Yet, the pore distribution increases due to the aggregation of formed nanoparticles. The decrease in specific surface area of Pt/HTNs relative to the support HTNs is probably due to a clogging of pores by Pt. The same phenomenon was observed for the Pt/HTNs-cal.

3.4. Electrochemical performance of catalysts

Typical examples of cyclic voltammograms of platinum in acid medium are outlined in Fig. 6. On both voltammograms, three regions are observed as described in the literature [30,31]:

- The region of hydrogen (H_{ads}, H_{des}) which corresponds to the hydrogen adsorption–desorption from −0.2 to 0.1 V *vs.* SCE,
- The region of the double layer (DL, form 0.1 to 0.35 V *vs.* SCE) wherein the residual current is a capacitive current. Afterward, the oxygen region (O: Oxide formation) which corresponds to the oxidation of the metal surface by chemisorption of oxygen species (OH_{ads}, … O_{ads}). Finally, when the scan is reversed, the current becomes negative with the appearance of a desorption peak of oxygen species (O′: Oxide reduction) which was chemisorbed during the anodic scan to 0.5 V *vs.* SCE.

Estimations of the electrochemically active surface areas (EASA) of Pt/HTNs and Pt/HTNs-cal catalysts were determined from cyclic voltammograms (Fig. 6) by measuring the charge of the hydrogen desorption peaks after subtracting that of the double-layer region. For this, we assume that the charge corresponding to the adsorption of a monolayer of hydrogen on Pt is 210 μC cm^{-2} [32]. The active surface areas of catalysts ($EASA_{Pt}$) were calculated with the formula $EASA_{Pt} = Q_H/0.21$ [33]. The active surface area of the Pt/HTNs catalyst, which is determined by the charge corresponding to the hydrogen adsorption–desorption peaks depends mainly on the Pt particles size and surface orientation namely Pt (111), Pt (110) and Pt (100) facets. The current densities in the present work were obtained by dividing the current by the EASA. In Table 3 are listed for the three electrodes (the Pt/HTNs, Pt/HTNs-cal and Pt/C), the specific surface area of electrodes, the electrochemically active surface area (EASA) and the current densities (j/mA cm^{-2}) corresponding to the maximum oxidation peak of methanol.

As the CO species are the main poisoning intermediate during methanol electro-oxidation, a good catalyst should possess

Table.2
Texture of the different TiO_2-based support.

Samples	S_{BET} ($m^2 g^{-1}$)	Pore volume ($cm^3 g^{-1}$)	Average pore size (nm)
Titanium dioxide (Degussa P25)	43	–	–
HTNs	246	0.54	8.9
HTNs-cal	60	0.3	20
Pt/HTNs	147	0.31	8.6
Pt/HTNs-cal	46	0.18	15.3

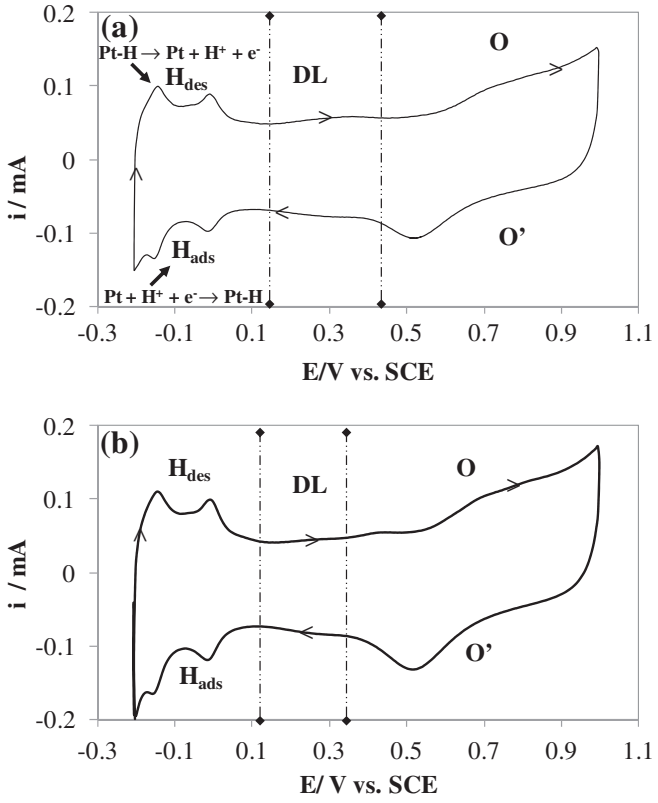

Fig. 6. Cyclic voltammograms of catalysts in 0.5 M H_2SO_4 recorded at 50 mV s^{-1} and room temperature: (a) Pt/HTNs and (b) Pt/HTNs-cal. The current was normalized with the EASA of Pt.

excellent CO electro-oxidation ability, which can be verified by CO stripping measurements [34,35]. The oxidation of pre-adsorbed carbon monoxide (CO) was measured by CO stripping voltammetry in 0.5 M H_2SO_4 solution at a scan rate of 20 mV s^{-1}. In Fig. 7 are presented CO stripping curves of Pt/HTNs, Pt/HTNs-cal and Pt/C catalysts. Different catalytic behaviors can be observed. As can be seen, the CO oxidation potential of Pt/HTNs catalyst begins from 0 V/SCE, which is lower than that of Pt/HTNs-cal (0.12 V/SCE) and Pt/C (0.4 V/SCE) catalysts.

These results demonstrated that Pt/HTNs catalyst can oxidize CO more easily at lower potential than Pt/HTNs-cal and Pt/C catalysts; this is explained by the activation of oxygen species by HTNs at potentials lower than on platinum. These oxygen species are necessary to carry out the oxidation of CO to CO_2 at low potential, which is helpful for releasing the active sites of Pt at low potential for further oxidation of methanol in direct methanol fuel cell (DMFC). Indeed, the impregnation method used for synthesizing platinum nanoparticles is very dependent on the nature of the substrate, and results in important variations of the platinum specific surface. The improvement of the synthesis method could lead to a better correlation between CO_{ads} oxidation experiment and methanol oxidation.

Table 3
Characterization of platinum based electrodes and performance for methanol oxidation reaction.

Electrodes	Pt/C XC72	Pt/HTNs	Pt/HTNs-cal
Specific surface area (m^2 g^{-1})	20	21	21
$EASA_{Pt}$ (cm^2)	0.59	0.79	0.74
j/mA cm^{-2}	1.32	3	2.35

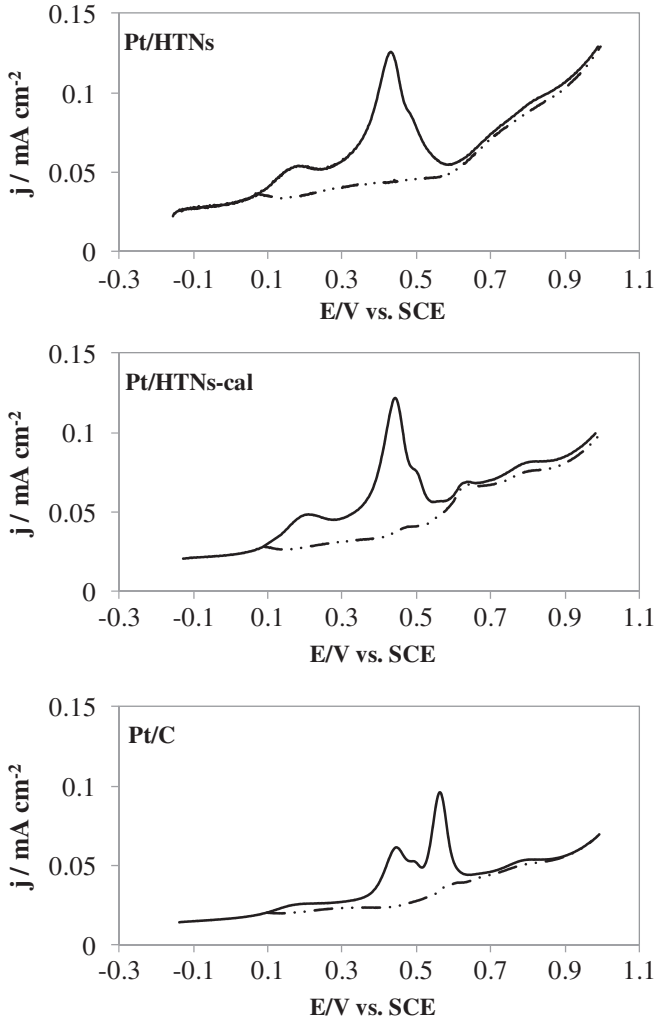

Fig. 7. CO stripping positive scan (solid line) of different catalysts in 0.5 M H_2SO_4 recorded at 20 mV s^{-1} and room temperature. The current was normalized by the EASA of Pt.

3.5. Cyclic voltammetry in presence of methanol in acidic solution

Fig. 8 shows the voltammograms of Pt/HTNs, Pt/HTNs-cal, Pt/C electrodes in methanol acidic solution (1 M CH_3OH + 0.5 M H_2SO_4). During the potential sweep in the positive direction, the anodic current for oxidation of methanol appears at 0.2 V and leads to a

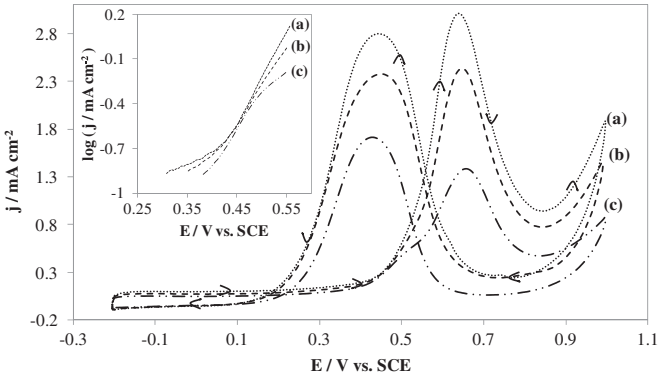

Fig. 8. Cyclic voltammograms of catalysts in 0.5 M H_2SO_4 in presence of 1 M CH_3OH recorded at 50 mV s^{-1} and room temperature: (a) Pt/HTNs; (b) Pt/HTNs-cal; (c) Pt/C. The current was normalized by the EASA of Pt.

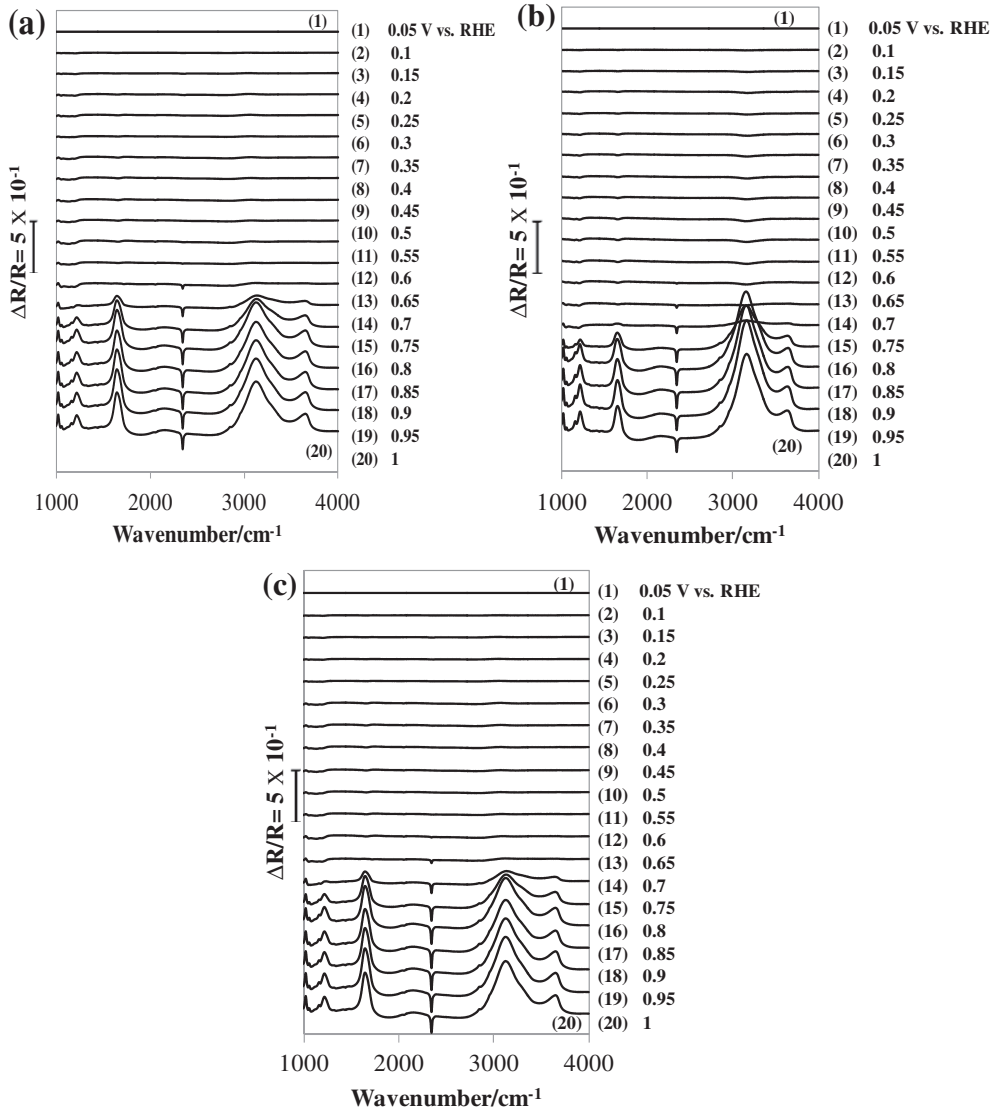

Fig. 9. In situ FTIR spectra recorded during the electro-oxidation of 1 M methanol in 0.5 M H_2SO_4 of catalysts: (a) Pt/HTNs, (b) Pt/HTNs-cal and (c) Pt/C as function of the increasing potential steps from 0.05 V to 1.00 V vs. RHE. The reference spectrum was collected at 0.05 V vs. RHE.

broad peak near 0.62 V. This phenomenon is in good agreement with the observation in the literature [36,37]. After this peak, the decrease of current density is attributed to the formation of oxides on the surface of the electrode leading to a non-active surface. During the negative sweep, another anodic current density peak appears at the potential of 0.44 V. It reflects the desorption of oxygenated species from the surface of Pt, which is then able to perform again the catalysis of the electro-oxidation of methanol.

Table.4
The characteristic IR peaks for methanol and the possible products.

Compound	IR band cm^{-1}
CO_2	2330–2365
CO (linear)	2010–2067
C–O–C	1160
–COOH	1780
–CHO	1450
$-OCH_3$	2815–2830
–HOH	1640
HSO_4^-	1217

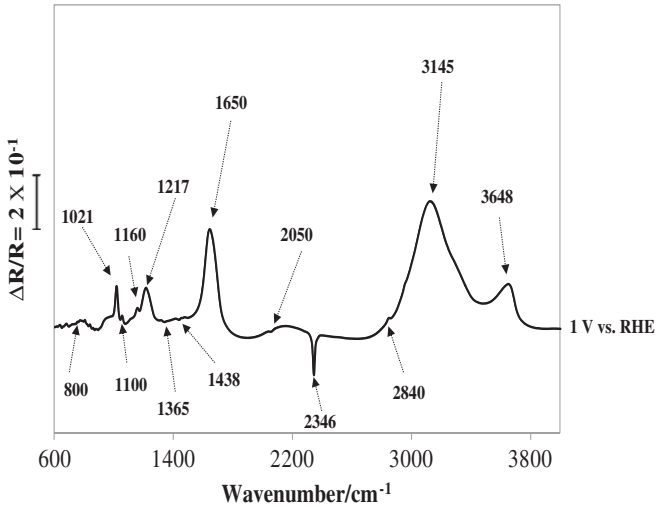

Fig. 10. In situ FTIR spectra of the adsorbates resulting from the chemisorption of methanol on a Pt/HTNs electrode during the electro-oxidation of 1 M methanol in 0.5 M H_2SO_4. The reference spectrum was collected at 0.05 V vs. RHE.

As shown in the inset graph of Fig. 8, log (j) vs. E, it is clear that the oxidation of methanol begins 100 mV earlier on the Pt/HTNs than Pt/C catalyst. The small size in diameter of HTNs and their higher specific surface area, could contribute to this performance. The performance of Pt/HTNs catalysts is better than that of the two other catalysts at high current densities. The current densities corresponding to the peak of the maximum oxidation on Pt/HTNs, Pt/HTNs-cal and Pt/C electrodes are listed in Table 3.

3.6. In situ infrared reflectance spectroscopy measurements of different catalysts

Fig. 9 shows FTIR spectra for the oxidation on different catalysts of 1 M of methanol in 0.05 M H_2SO_4. The spectra were taken in the 1000–4000 cm^{-1} spectral range, between 0.05 and 1.4 V *vs*. RHE, at 0.05 V intervals during a linear voltammetry carried out at 1 mV s^{-1}. IR spectra were calculated for each potential value as

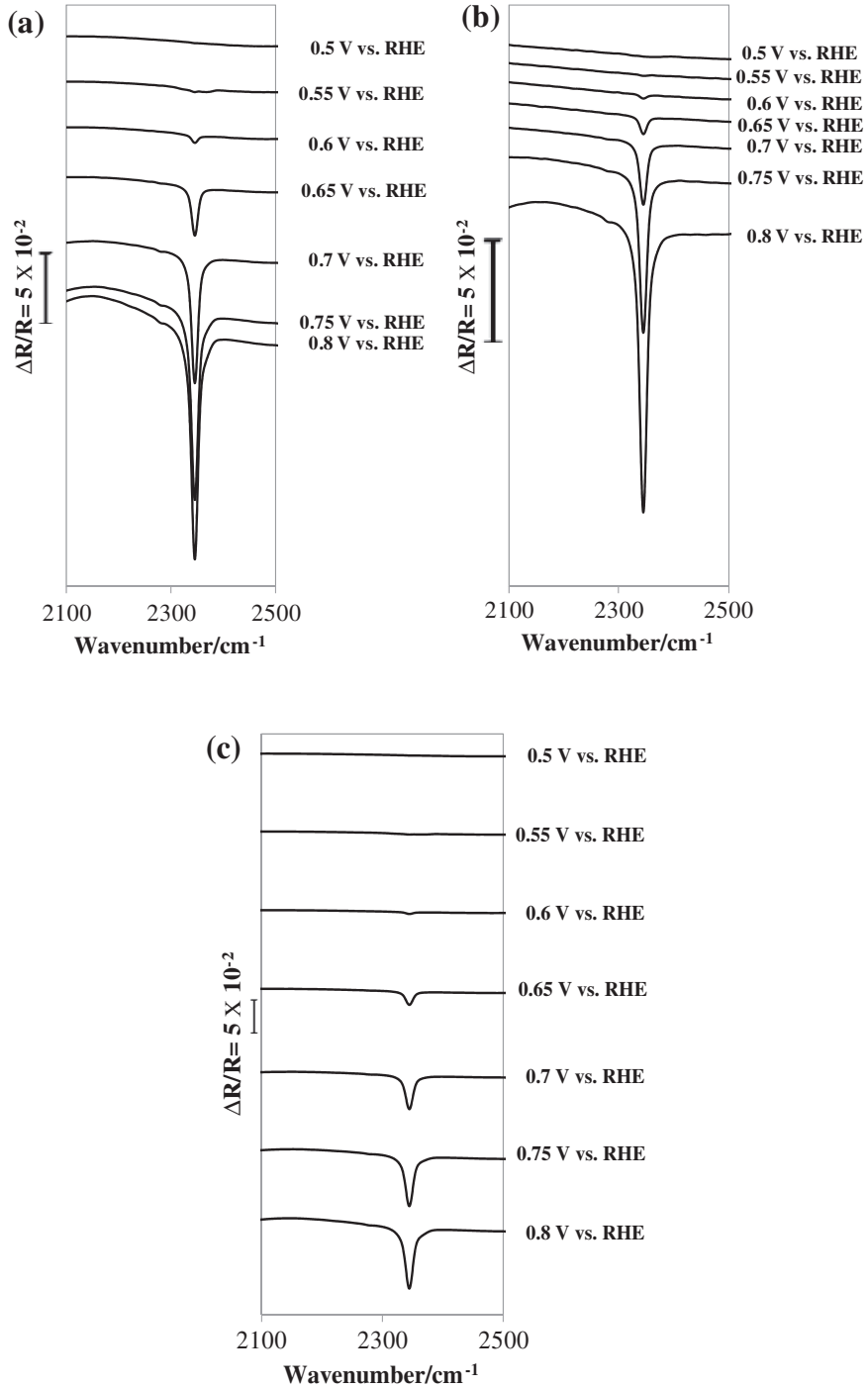

Fig. 11. In situ FTIR spectra on the appearance of the band of CO_2 recorded during the electro-oxidation of 1 M methanol in 0.5 M H_2SO_4 of catalysts: (a) Pt/HTNs, (b) Pt/HTNs-cal and (c) Pt/C. The reference spectrum was collected at 0.05 V vs. RHE.

changes in the reflectivity (R) relative to a reference single-beam spectrum (R_{ref}) as:

$$\Delta R/R = \left(R_{E_i} - R_{E_{ref}}\right) \Big/ R_{E_{ref}} \quad (3)$$

where E_i is the potential at which the accumulation is carried out and E_{ref} is the reference potential corresponding to 0.05 V and 1.05 V *vs*. RHE when following the vibrations of CO and CO_2, respectively. For better readability of the spectra, each spectrum was shifted to a constant value $\Delta R/R$. In this case, a negative peak means the production of species such as CO_2 and a positive absorption band indicates the consumption of species at the electrode surface such as CO.

In general, the FTIR spectra of different catalysts were similar Fig. 9(a–c) and provided information about adsorbed intermediates (linearly bonded CO) and one of the reaction products (CO_2). The interaction of methanol with HTNs surface does not produce important modifications of the alcohol spectrum. The peaks are assigned according to the vibration frequencies of methanol and possible related products as collected in Table 4 [38–43].

Hence, as an example, the last FTIR spectrum (at 1.0 V *vs.* RHE) recorded during methanol electro-oxidation on Pt/HTNs (Fig. 10) is explained here in detail. The broad band from 800 cm^{-1} was assigned to Ti–O and Ti–O–Ti frequency region.

A positive band is observed around 1021 cm^{-1}, which is attributed to the loss of methanol and/or formaldehyde that have the same characteristic vibration peak at 1021 cm^{-1}. Because formaldehyde can be further oxidized in the cell at higher potential, the amount of formaldehyde is lower than that of consumed methanol. Therefore the peak converts to upward, and reflects the depletion of methanol in the reaction. The downward peak at 1100 cm^{-1} can be attributed to $CH_2(OCH_3)_2$.The downward peak at 1160 cm^{-1} has the possibility to be both the νas_{C-O} (νas is the asymmetric vibration) of formate species –HCO–O– in $HCOOCH_3$ or in the ether species C–O–C. Considering the similarity of the potential dependence with the methoxy $-OCH_3$ species, the peak around 1160–

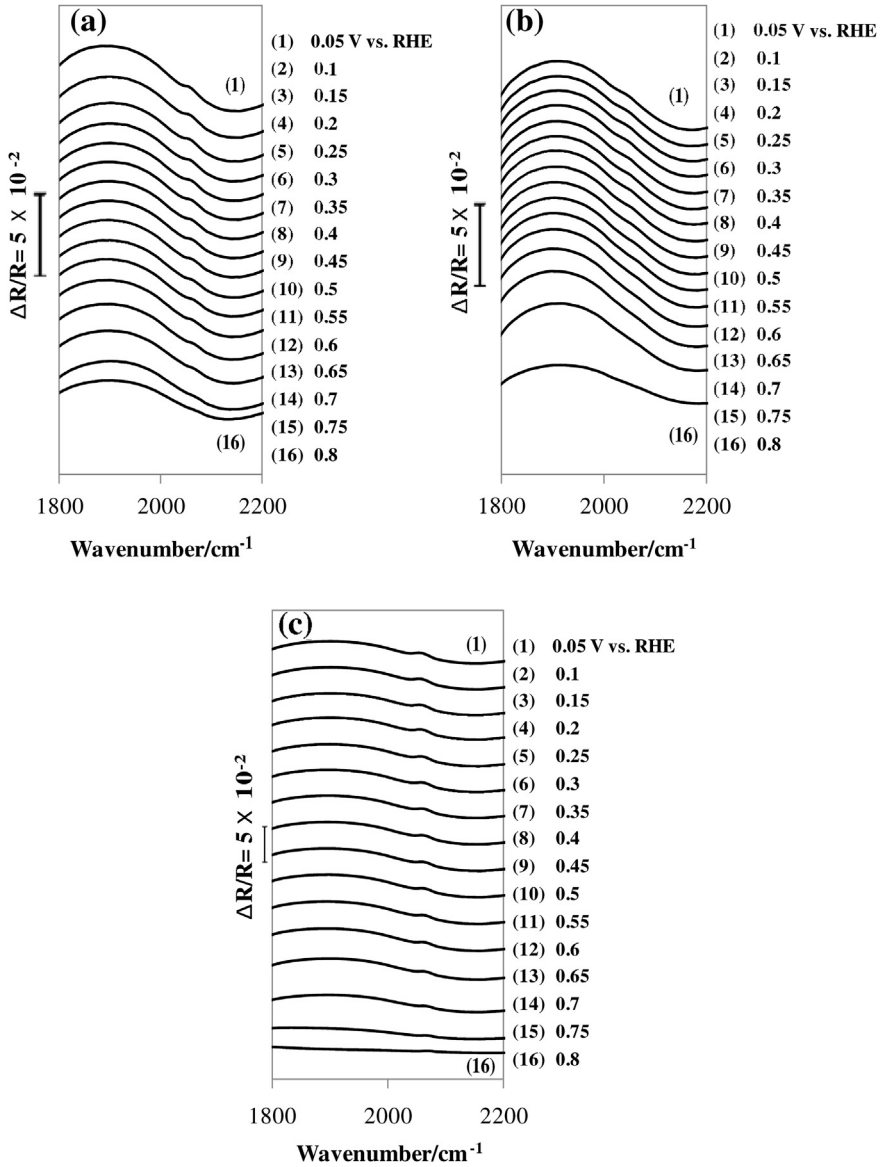

Fig. 12. Potential dependence of the CO_L band in 1 M methanol in 0.5 M H_2SO_4 of catalysts: (a) Pt/HTNs, (b) Pt/HTNs-cal and (c) Pt/C. The reference spectrum was collected at 1.05 V vs. RHE.

1190 cm^{-1} has been assigned to the νas_{C-O} of the formate species −HCO−O− in $HCOOCH_3$. The vibration at 1217 cm^{-1} corresponds to HSO_4^- species in the sulfuric acid solution. The peak at 1365 cm^{-1} can be assigned to the vibration for formic acid.

For potential values higher than 0.6 V an upward peak at 1650 cm^{-1} appears, which is assigned to the ν_{OH} vibration of water. The intensity of this peak increases with increasing potentials, which indicates the depletion of H_2O in the monolayer during the oxidation reaction of methanol. This depletion is confirmed by the upward peak in the wavenumber region 3100–3500 cm^{-1}, which corresponds to both the ν_{OH} vibration of methanol and ν_{OH} vibration of water. The upward peak 2840 cm^{-1}, is assigned to the degenerate stretching vibration of CH_3 for methoxy $-OCH_3$ species of methanol.

A single downward peak appears at 2346 cm^{-1} that is assigned to the anti-symmetric stretching vibration of dissolved CO_2 in aqueous solution. The intensity of the CO_2 peak increases with increasing potential, which indicates the accumulation of product CO_2 in the solution close to electrode at high potential.

As can be seen in Fig. 11, for potential values higher than 0.5 V *vs* RHE, the IR band corresponding to CO_2 is more intense and appears earlier for Pt/HTNs (Fig. 11a) when compared with Pt/HTNs-cal and Pt/C catalysts (Fig. 11b, c). We can therefore conclude that the Pt/HTNs catalyst oxidizes CO to CO_2 at lower potential compared to Pt/HTNs-cal and Pt/C.

Fig. 12 (a, b and c) shows FTIR spectra for oxidation on different catalysts of 1 M of methanol in 0.05 M H_2SO_4 recorded between 1800 cm^{-1} and 2200 cm^{-1}. The absorption band located to 2053 cm^{-1} is assigned to the vibration of linearly bonded (CO_L) adsorbed CO on the surface of platinum.

The CO_L band appears in the first potential to 0.05 V *vs*. RHE, indicating that methanol chemisorption to form adsorbed CO takes place at very low potentials. The intensity of this band starts to decrease at 0.7 V *vs*. RHE, correlated to the appearance of the band CO_2.

According to the results obtained from cyclic voltammetry and in situ FTIR, the mechanism of methanol oxidation process in aqueous media can be analyzed. As the potential increases, the products HCHO, HCOOH, $HCOOCH_3$ and $CH_2(OCH_3)_2$ can be formed via possible pathways, as shown in Fig. 13.

The adsorbed intermediate CO species could be formed by the reaction and it can be further oxidized into CO_2.

$$CH_3OH + Pt \rightarrow Pt\text{-}CO + 4H^+ + 4e^- \quad (4)$$

$$Ti + H_2O \rightarrow Ti\text{-}OH + H^+ + e^- \quad (5)$$

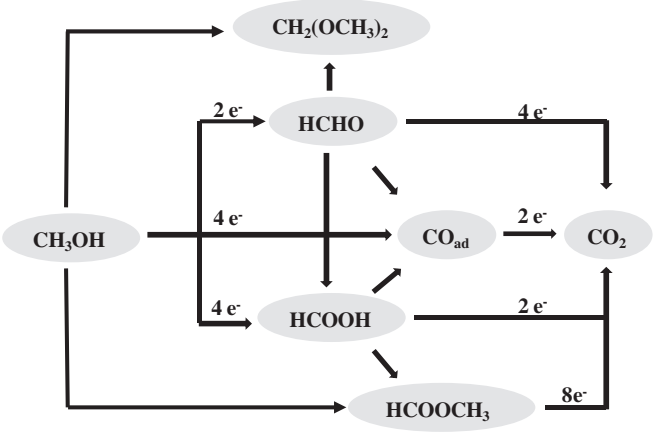

Fig. 13. Reaction pathways of methanol oxidation at a Pt surface.

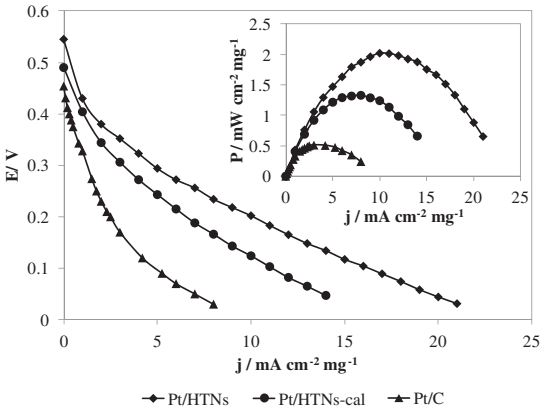

Fig. 14. Polarization curves of direct methanol fuel cell at 90 °C using different anodes catalysts: Pt/HTNs, Pt/HTNs-cal and Pt/C. Pt/C cathode was used and the current density and the power density were normalized by the geometric surface area of the cell and the Pt weight at the anode.

$$Ti\text{-}OH + Pt\text{-}CO \rightarrow Pt + Ti + H^+ + CO_2 + e^- \quad (6)$$

The surface of the hydroxylated Ti facilitates the adsorption of oxygenated species. It is widely accepted that active oxygen-contained surface species are necessary to the oxidative removal of CO poisoning intermediates on Pt surface [44].

The overall reaction for the electrochemical oxidation of methanol in acid aqueous solution is:

$$CH_3OH + H_2O \rightarrow 6H^+ + 6e^- + CO_2 \quad (7)$$

3.7. Operation of direct methanol fuel cell

Based on the above results, polarization curves were obtained for the DMFC single-cell that used Pt/HTNs or Pt/HTNs-cal (metal loading of 1.5 mg cm^{-2}) and Pt/C (metal loading of 2 mg cm^{-2}) as anodes electrodes.

Pt/C as cathode material (metal loading of 1 mg cm^{-2}) (Fig. 14). The system operated at 90 °C. The current density and the power density were normalized by mass of platinum.

In these conditions, the open circuit voltage obtained for the system with Pt/HTNs-cal, Pt/C anodes are about 0.49 V and 0.45 V respectively. These values of open circuit voltage are closed to those usually obtained in the literature [45]. An increase of this value to 0.54 V was observed with Pt/HTNs. This value is low and can be due to the strong adsorbed species at the anode surface. During the operation, higher current densities can be reached with this anode is 21 mA cm^{-2} mg^{-1}. A maximum power density of 2 mW cm^{-2} mg^{-1} was observed at 11 mA cm^{-2} mg^{-1}. This performance is low when it is compared to that of Pt-based catalysts in the literature. However, these results show the application of these electrodes for such a system.

During, the electro-oxidation of methanol, various adsorbates such as, (HCHO), carboxy (−COOH), or (HCOO−) have been proved to be the reactive intermediates, but it is evident that the CO species reacted as poison of the Pt catalyst. We demonstrate that Pt/HTNs preferentially oxidizes CO poisoning species that are produced during operation of the DMFC.

4. Conclusions

The results presented in this study indicated that the catalytic activities of Pt/HTNs catalysts for methanol electro-oxidation were greatly improved due to the structure of HTNs, and a promising

direction for developing anode catalysts for methanol oxidation. The TEM and XRD showed that the prepared HTNs have uniform length and diameter distribution. Studies of adsorption isotherms showed a higher specific surface area for hydrogenotitanates nanotubes which is suitable for a good dispersion of electrocatalysts. The CV demonstrated that the Pt/HTNs catalysts have higher catalytic activity and better stability for methanol electro-oxidation. The corresponding CO stripping potential shifted to lower direction than Pt/HTNs-cal and Pt/C catalysts, indicating that HTNs can enhance CO electro-oxidation, which is helpful for methanol electro-oxidation.

The application of in situ transmission difference FTIR spectroscopy method for study on the anodic oxidation of methanol in aqueous solution has been demonstrated. It was found that methanol could be oxidized into formaldehyde, formic acid, methyl formate and dimethoxymethane, and it could be further oxidized into CO_2. The adsorbed CO as the poisoning intermediate was also detected. Experimental results on methanol oxidation show that this method has the ability to clarify the identity of species involved in the oxidation process both dissolved in solution and adsorbed at the surface of electrode. Performance of the DMFC is also improved with Pt/HTNs catalyst.

References

[1] J.M. Leger, S. Rousseau, C. Coutanceau, F. Hahn, C. Lamy, Electrochim. Acta 50 (2005) 5118–5125.
[2] V. Baglio, A.S. Arico, A. Di Blasia, V. Antonucci, P.L. Antonucci, S. Licoccia, E. Traversa, F. Serraino Fiory, Electrochim. Acta 50 (2005) 1241–1246.
[3] C. Grolleau, C. Coutanceau, F. Pierre, J.M. Leger, Electrochim. Acta 53 (2008) 7157–7165.
[4] H.J. Kim, D. Kim, H. Han, Y. Shul, J. Power Sources 159 (2006) 484–490.
[5] G. Wu, T. Chen, X. Zong, H. Yan, G. Ma, X. Wang, Q. Xu, D. Wang, Z. Lei, C. Li, J. Catal. 253 (2008) 225–227.
[6] M.B. Ji, Z.D. Wei, S.G. Chen, X.Q. Qi, L. Li, Q. Zhang, C. Liao, R. Tang, Int. J. Hydrogen Energy 34 (2009) 2765–2770.
[7] S.L. Gojković, J. Electroanal. Chem. 573 (2004) 271–276.
[8] V. Selvaraj, M. Alagar, Electrochem. Commun. 9 (2007) 1145–1153.
[9] I.Á. García, C. Ramírez, J.M. Hallen López, E.M. Arce Estrada, J. Alloys Compd. 495 (2010) 462–465.
[10] H. Ren, M.P. Humbert, C.A. Menning, J.G. Chen, Y. Shu, U.G. Singh, W. Cheng, Appl. Catal. A 375 (2010) 303–309.
[11] W. Vogel, J. Phys, Chem. C 112 (2008) 13475–13482.
[12] V. Neburchilov, H. Wang, J. Zhang, Electrochem. Commun. 9 (2007) 1788–1792.
[13] N. Rajalakshmi, N. Lakshmi, K.S. Dhathathreyan, Int. J. Hydrogen Energy 33 (2008) 7521–7526.
[14] H. Yuana, D. Guo, X. Qiu, W. Zhu, L. Chen, J. Power Sources 188 (2009) 8–13.
[15] T. Kasuga, M. Hiramatsu, A. Hoson, T. Sekino, K. Niihara, Adv. Mater. 11 (1999) 1307–1311.
[16] G. Guo, C. He, Z. Wang, F. Gu, D. Han, Talanta 72 (2007) 1687–1692.
[17] B. Zhao, F. Chen, H. Liu, J. Zhang, J. Phys. Chem. Solids 72 (2011) 201–206.
[18] M. Cruza, J. Solísa, R. Zanella, Catal. Today 166 (2011) 172–179.
[19] C. Lee, C. Wang, M. Lyu, L. Juang, S. Liu, S. Hung, J. Colloid Interface Sci. 316 (2007) 562–569.
[20] C. Tsai, H. Teng, Chem. Mater. 18 (2006) 367–373.
[21] H. Song, X. Qiu, X. Li, F. Li, W. Zhu, L. Chen, J. Power Sources 170 (2007) 50–54.
[22] P. Xiao, H. Songa, X. Qiua, W. Zhua, L. Chen, U. Stimming, P. Bele, Appl. Catal. B 97 (2010) 204–212.
[23] H. Kochkar, A. Turki, L. Bergaoui, G. Berhault, A. Ghorbel, J. Colloid Interface Sci. 331 (2009) 27–31.
[24] H. Kochkar, N. Lakhdhar, G. Berhault, M. Bausach, A. Ghorbel, J. Phys. Chem. C 113 (2009) 1672–1679.
[25] A. Turki, H. Kochkar, G. Berhault, A. Ghorbel, Stud. Surf. Sci. Catal. 175 (2010) 593–596.
[26] M. Qamar, C.R. Yoon, H.J. Oh, N.H. Lee, K. Park, D.H. Kim, K.S. Lee, W.J. Lee, S.J. Kim, Catal. Today 131 (2008) 3–14.
[27] J. Yang, Z. Jin, X. Wang, W. Li, J. Zhang, S. Zhang, X. Guo, Z. Zhang, Dalton Trans. (2003) 3898–3901.
[28] G. Mogilevsky, Q. Chen, A. Kleinhammes, Y. Wu, Chem. Phys. Lett. 460 (2008) 517–520.
[29] J. Lynch (Ed.), Analyse physico-chimique des catalyseurs industriels, Manuel pratique de caractérisation, Technip, (2001).
[30] L.D. Burke, D.T. Buckley, J. Electroanal. Chem. 405 (1996) 101–109.
[31] F.A. Bruijn, B.F.M. Kuster, G.B. Marin, Appl. Catal. A 145 (1996) 351–374.
[32] C. Naour, Thesis, Université de Paris XI, (1994).
[33] X.S. Peng, K. Koczkur, S. Nigro, A.C. Chen, Chem. Commun. 24 (2004) 2872–2873.
[34] M. Wang, D. Guo, H. Li, J. Solid State Chem. 178 (2005) 1996–2000.
[35] S. Thomas, X. Ren, S.J. Gottesfeld, J. Electrochem. Soc. 146 (1999) 4354–4359.
[36] H. Song, X. Qiu, F. Li, Electrochim. Acta 53 (2008) 3708–3713.
[37] B. Abida, L. Chirchi, S. Baranton, T.W. Napporn, H. Kochkar, J.M. Léger, A. Ghorbel, Appl. Catal. B 106 (2011) 609–615.
[38] B. Beden, F. Largeaud, K.B. Kokoh, C. Lamy, Electrochim. Acta 41 (1996) 701–709.
[39] Y. Zhu, H. Uchida, Y. Takahiro, T. Fujino, M. Watanabe, Langmuir 17 (2001) 146–154.
[40] B. Beden, C. Lamy, N.R. Tacconi, A. Arvia, J. Electrochim. Acta 35 (1990) 691–704.
[41] A. Kabbabi, R. Faure, R. Durand, B. Beden, F. Hahn, J.M. Leger, C. Lamy, J. Electroanal. Chem. 444 (1998) 41–53.
[42] Y. Liu, M. Muraoka, S. Mitsushima, K.I. Ota, N. Kamiya, Electrochim. Acta 52 (2007) 5781–5788.
[43] D. He, L. Yang, S. Kuang, Q. Cai, Electrochem. Commun. 9 (2007) 2467–2472.
[44] C. Lamy, A. Lima, V. Lerhun, F. Delime, C. Coutanceau, J.M. Léger, J. Power Sources 105 (2002) 283–296.
[45] S. Beyhan, J.M. Léger, F. Kadırgan, Appl. Catal. B: Environ. 130–131 (2013) 305–313.